Journal of Engineering Science *Vol. XXVIII, no. 2 (2021), pp. 25 - 33*
Fascicle *Industrial Engineering* *ISSN 2587-3474*
Topic *Materials Science and New Technologies* *eISSN 2587-3482*

https://doi.org/10.52326/jes.utm.2021.28(2).01
UDC 535.012

OPTICAL ANISOTROPY AND BIREFRINGENCE OF $CuAlS_2$ CRYSTALS

Alisa Maşnic[1*], Victor Zalamai[2], Veaceslav Ursaki[2]

[1]*Technical University of Moldova, Stefan cel Mare pr. 168, Chisinau, MD-2004 Republic of Moldova*
[2]*National Center for Materials Study and Testing, Technical University of Moldova, Chisinau, MD-2004 Moldova*
*Corresponding author: Alisa Maşnic, *alisa.masnic@tlc.utm.md*

Received: 27.03.2021
Accepted: 06.05.2021

Abstract. Optical spectra were investigated in a spectral range of (300 - 700) nm for $CuAlS_2$ single crystals. Transmission and wavelength modulated transmission spectra demonstrated presence of some impurity absorption bands in the region of optical transparency of crystals. Optical functions (real and imaginary components of the dielectric function, refractive index and extinction coefficient) have been calculated from the optical reflection spectra by means of the Kramers-Kronig relations. A strong anisotropy and birefringence have been revealed for $CuAlS_2$ crystals. Two isotropic points have been found in (100) oriented platelets around 380 nm and 530 nm. The position of the isotropic point around 530 nm was found to be strongly influenced by the technological conditions of crystal growth and platelet thickness, it being situated at 535 nm for a platelet with thickness of 223 μm. An optical band-pass filter was constructed with such a platelet placed between two Gran-Thompson prism crossed polarizers.

Keywords: *transmission spectra; optical constants; birefractive effects; $A^IB^{III}C^{VI}_2$ chalcopyrite compounds; isotropic point.*

1. Introduction

$A^{II}B^{VI}$ compounds are widely used in electronic, optoelectronic and photonic devices [1, 2]. $A^IB^{III}C^{VI}_2$ compounds can be considered as an extension of the zincblende $A^{II}B^{VI}$ materials from the point of view of their crystal structure, they being an alternative stack of two zincblende cells with two cations A^I and B^{III} instead of the A^{II} cation. This results in a non-centro symmetrical structure with anisotropy of optical properties. Particularly, especial interest presents the birefringence inherent to these materials, making them suitable for the developments of optical filters [3 - 12], in addition to their use in solar cells [13 - 15], light-emitting devices [16, 17], photo catalysis [18, 19] and nonlinear optics [20].

It should be noted that optical activity is inherent to most of the birefringent crystals. According to the crystal symmetry, 15 point groups of crystal from the total amount of 32 ones exhibit optical activity, and only two of these 15 point groups with optical activity do not exhibit birefringence [21]. Therefore, the chalcopyrite crystals belonging to the - 42 m point group have both birefringence and optical activity. Usually, the phase difference induced by birefringence is much larger as compared to the phase difference caused by optical activity.

Some of $A^{I}B^{III}C^{VI}_2$ chalcopyrite compounds are suitable for the fabrication of band pass or band elimination filters with narrow enough band. The existence of accidental isotropy and isotropic wavelengths at which the ordinary and extraordinary refractive indexes are equal to each other is a necessary condition for uniaxial anisotropic crystals to be suitable for the preparation of such filters. Particularly, band elimination filters are very useful for applications in Raman spectroscopy, allowing one measuring of Raman scattering at frequencies much closer to the excitation line, even with single monochromators, instead of using much more expensive double or triple monochromators. Particularly, optical band pass filters on the basis of optically active uniaxial crystal of $AgGaSe_2$ were proposed for Raman spectroscopy with AlGaAs semiconductor lasers [7 - 10].

Horinaka et al. proposed a criterion of applicability of chalcopyrite semiconductors to optical line elimination filters on the basis of the analysis of contribution of anisotropy of transition intensity to birefringence [22]. It was found that the effect of the lowest direct band-gap E_g to the birefringence is proportional to $E_g^{-1.5}$. On the other hand, the birefringence at longer wavelengths is influenced by the average effect of various bad-gaps, and it depends on the lattice strain (1-c/2a). The compounds were divided into three groups according their position on a plot of $E_g^{-1.5}$vs– (1 -c/2a). The compound located at small values of $E_g^{-1.5}$ and large values of $|(1 - c/2a)|$ were suggested to have a high probability of possessing accidental isotropic wavelength. According to this analysis, all the compounds with Cu and In, as well as most of compounds with Teshould not possess accidental isotropic wavelength. All the compounds with Ag, Al, Se and those with Ag, Ga, Se should have the accidental isotropic wavelength. As concerns crystals with Cu and Al or Ga and Se or S, it was predicted that the compounds $CuAlS_2$, $CuAlSe_2$, and $CuGaS_2$ should have accidental isotropic wavelength, while the $CuGaSe_2$ should not. On the other hand, it was experimentally found that indeed $CuGaSe_2$ does not have accidental isotropic wavelength, while $CuAlSe_2$, and $CuGaS_2$ do have it. As concerns $CuAlS_2$ crystals the situation renamed uncertain.

The goal of this paper is to investigate the optical anisotropy and birefringence of $CuAlS_2$ crystals, and to explore possibilities of constructing optical filters on their basis.

2. Experimental details

$CuAlS_2$ crystals in the form of platelets with 2.5×1.0 cm^2 mirror-like surfaces and thicknesses of 300-400 μm have been grown by chemical vapor transport, and thin layers in the form of rectangular prisms were cut from bulk crystals. The prisms with the thickness *l* varying from 15 μm to more than 200 μm were crystallographic oriented with (100) faces and with the c-axis in this plane. These rectangular prisms of birefringent and optically active crystals have been mounted between a polarizer and an analyzer (Glan-Thomson polarization prisms) as shown in Figure 1. The x, y coordinates of the optical system correspond to the polarizer and analyzer axes and the z-

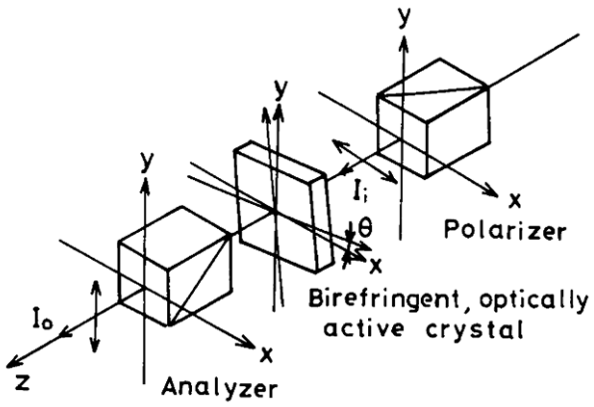

Figure 1. Optical arrangement for measurement of filter characteristics.

axis is taken to be the light propagation direction. The incident (100) face of the crystal prism is perpendicular to the z-axis, while the principal axes of the dielectric tensor form an Θ angle with the x and y axes.

In such a system, the ratio of the light intensity behind the analyzer I_o to the intensity of the intensity of light passed through the polarizer I_i is given by [21]:

$$\frac{I_0}{I_i} = E(\lambda, \theta) \cdot R(\lambda), \tag{1}$$

$$E(\lambda, \theta) = \frac{\delta_b^2 sin^2 2\theta + \delta_g^2}{\delta_b^2 + \delta_g^2}, \tag{2}$$

$$R(\lambda) = sin^2 \frac{(\delta_b^2 + \delta_g^2)^{1/2}}{2} \tag{3}$$

where $\delta_b = (2\pi/\lambda) l \cdot \Delta n$ is the retardation by birefringence, $\delta_g = (2\pi/\lambda)\, l(G/\bar{n})$ is the retardation by optical activity, Δn is the birefringence, G is the optical gyration and $\bar{n}$ is the average refractive index. $E(\lambda,\Theta)$ is treated as an anvelope of (I_o/I_i), since it is much less sensitive to the wavelength than $R(\lambda)$ is. When the Θangle is equal to zero, then the equation (2) becomes:

$$E(\lambda, 0) = \frac{\delta_g^2}{\delta_b^2 + \delta_g^2}. \tag{4}$$

Since Δn is equal to zero at the accidental isotropic wavelength λ_o and it rapidly increases toward both sides of the isotropic point, $E(\lambda,\Theta)$ will have characteristics of a band pass filter with the central wavelength at λ_o, and it will be equal to unity when Δn and $\delta_b$are equal to zero. $R(\lambda)$ also should be equal to unity at the isotropic wavelength in order (I_o/I_i) to reach a maximum. This will happen when the thickness l is chosen so that δ_g to acquire the value of $(2m+1)$, where m = 0, 1, 2, 3…The optical spectra were measured at room temperature with a double SDL-1 spectrometer as shown in Figure 2. The wavelength modulated spectra were measured with a MDR-2monochromator.

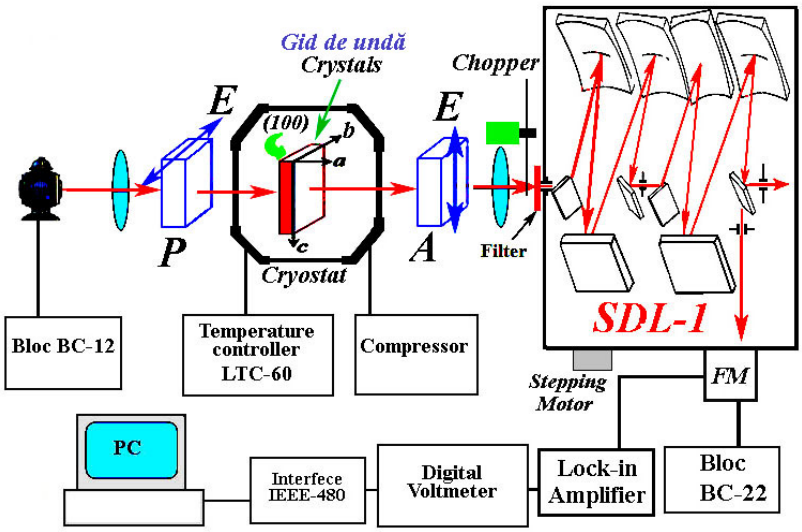

Figure2. Experimental set-up for transmission spectra measurements.

3. Experimental results and discussions

Figure 1 presents optical transmission spectra of $GuAlS_2$ crystals in E||c and E⊥c polarizations. Absorption bands a3 and a4 are observed in E⊥c polarization, as well as e3

and e4 in E||c polarization, respectively. Apart from that, a1 and a2 features are observed in E⊥c polarization. The transmission maxima are marked with m1 and m2. The slightly shift of the e3 and e4 points to shorter wavelengths with respect to the a3 and a4is an indication of anisotropy of optical properties of $GuAlS_2$ crystals. If the radiation with $\lambda=\lambda_0$ wavelength propagates through a crystal, the energy transfer occurs from the mode polarized as n_o (or n_e) to the mode polarized as n_e (or n_o), i.e. the interaction of two orthogonally polarized modes is revealed in the crystal's isotropic point.

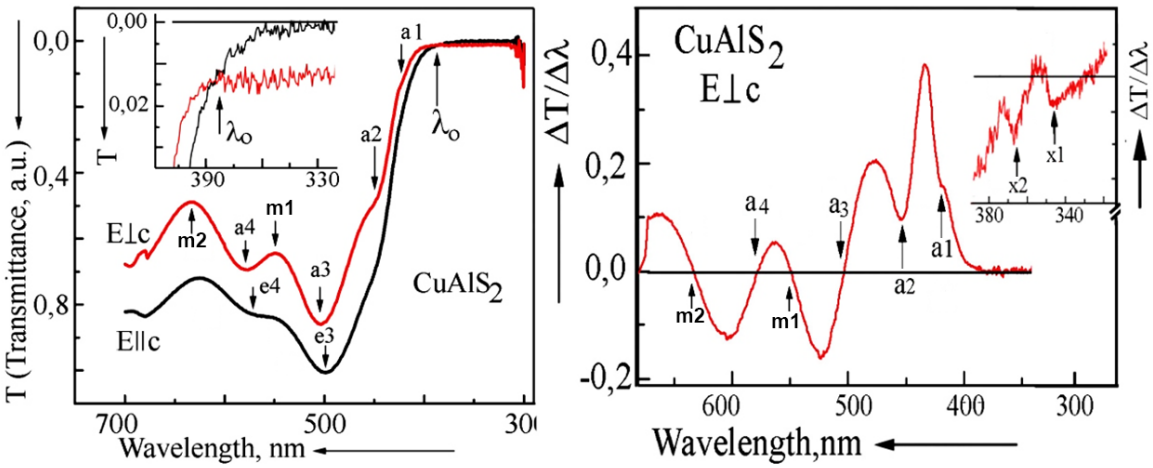

Figure 3. Transmission spectra anisotropy (left) and wavelength modulated transmission spectra (right) of $CuAlS_2$ single crystals with thickness of 223 μm.

Wavelength modulated spectrum was measured for a more precise determination of these features, since they are more pronounced in the wavelength modulated spectrum, actually corresponding to the first derivative of the transmission with respect to the wavelength. Two additional minima x1 and x2 are observed in wavelength modulated transmission spectrum. The minima a3 and a4, as well as the maxima m1 and m2 in the transmission spectrum correspond to points were the wavelength modulated spectrum intersects the abscise axis. The absorption bands a1 and a3 are not deep enough to lead to the intersection of the abscise axis. The absorption bands a1 – a4 are most probably due to some electron transitions to impurity levels, while the features x1 and x2 are in the region of fundamental absorption due to valence band to conduction band electron transitions. The wavelengths and photon energy of these features are presented in Table 1.

Table 1

The wavelengths and photon energy of features observed in Figure 1

Feature	a1	a2	a3	a4	m1	m2	x1	x2
Wavelength (nm)	420	450	500	580	550	630	348	368
Photon energy (eV)	2.98	2.76	2.45	2.14	2.25	1.97	3.56	3.37

The anisotropy of the absorption (transmission) edge in the region of fundamental absorption is determined by the direct allowed electronic transitions from the valence bands with Γ7 and Γ6 symmetry to the conduction band with Γ6 symmetry. While going away from the absorption edge towards the long wavelength region, the absorption magnitude is increasing sharper for E||c polarization than for the E⊥c polarization. As a result, the optical transmission curves measured in E||c and E⊥c polarizations intersect each

other at a wavelength around 380 nm as one can see from the inset in Figure 1 (left). This intersection occurs due to the presence of an isotropic point marked as λ_0 as discussed below in connection with the curves for the ordinary and extraordinary refractive indexes.

The anisotropy of optical properties of $CuAlS_2$ crystals is revealed from the investigation of spectral dependences of dielectric functions in E||c and E⊥c polarizations. The spectral dependences of the real ε_1 and imaginary ε_2 dielectric functions were calculated from experimental reflectivity spectra taking into account that

$$r = \frac{n-ik-1}{n-ik+1} = \sqrt{R}e^{i\varphi} \tag{5}$$

Where r is the complex reflectivity, R is the measured reflectivity, n is the real refractive index, k is the extinction coefficient and φ is the phase angle.

The phase angle is calculated according to the Kramers-Kronig relations as:

$$\varphi(\omega_0) = \int_0^{\infty} \frac{lnR(\omega)}{\omega_0^2-\omega^2} d\omega \tag{6}$$

Experimentally, the R is measured in a limited spectral range $a \leq \omega \leq b$. In our case measurements have been performed in a spectral range from 2.5 eV to 4.5 eV. In the high-energy region an approximation of the spectral dependence of the reflection coefficient is used to calculate the dielectric constants using an analytic function. We have used a simple approximation: $R(\omega) = R(a)$ for $a \leq \omega \leq b$ and $R(\omega) = c\omega^p$ for $b \leq \omega \leq \infty$, where c and p are constants according to [23].

By knowing the R and φ(ω) one can calculate the optical constants as

$$\varepsilon_1 = n^2 - k^2, \text{ and } \varepsilon_1 = 2nk, \tag{7}$$

Where

$$n = \frac{1-R}{1-2\sqrt{R}cos\varphi+R}, \qquad k = \frac{2\sqrt{R}sin\varphi}{1-2\sqrt{R}cos\varphi+R}. \tag{8}$$

The spectral dependences of the real ε_1 and imaginary ε_2 components of the complex dielectric function ε calculated from the reflectivity spectra using equation (7) for a $CuAlS_2$ platelet with thickness of 223 μm are shown in figure 4. The anisotropy of optical properties is clearly observed from the comparison of spectra for E||c and E⊥c polarizations.

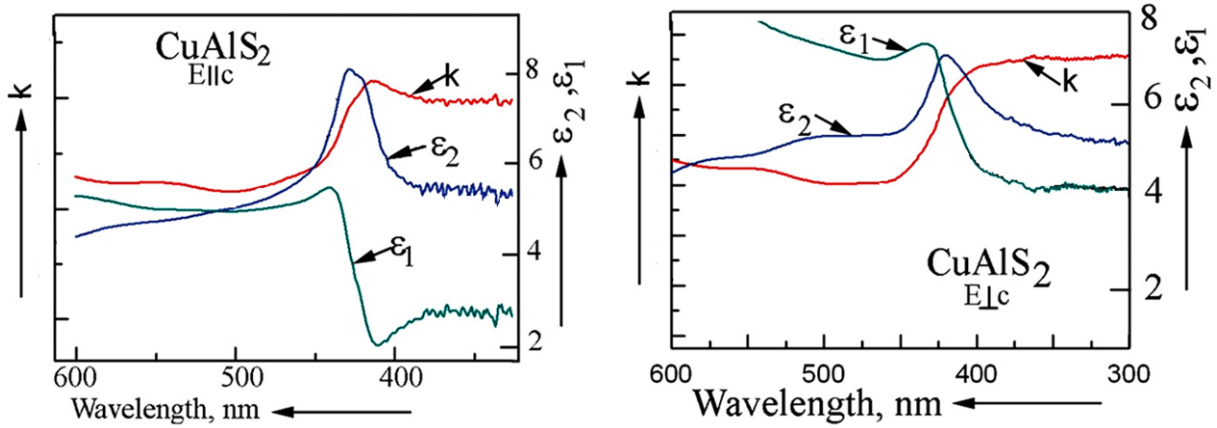

Figure 4. Spectral dependences of optical constants ε_1 ε_2, and k for polarizations E||c (left) and E⊥c (right) for $CuAlS_2$ crystals with thickness of 223 μm.

The spectral dependences of refractive indices for ordinary n_o and extraordinary n_e waves in $CuAlS_2$ crystals with thicknesses of 223 μm and 35 μm are compared in Figure 5. One can see that an isotropic wavelength $\lambda_0$is inherent to both crystals in the short wavelength, it being situated at around 380 nm in the 223 μm thick crystal, and at 375 nm in the 35 μm thick crystal. This value is close to the value of 378 nm previously reported for $CuAlS_2$ crystals [22]. Apart from this point, there is a second isotropic wavelength λ_{01} at longer wavelength. The difference in the position of this point is much more significant in crystal with different thickness, it being situated at around 535 nm in the 223 μm thick crystal, and at 485 nm in the 35 μm thick crystal. This difference is explained not only by the different gyroscopy in crystals with different thickness, but also may be influenced by different content and concentration of defects and impurities due to different technological condition of crystal growth. The crystal exhibits as negative birefringence ($n_e - n_o$) >0 at wavelengths higher than λ_0 and lower than λ_{01}, while it is positive at wavelengths between these two isotropic points $\lambda_{01}<\lambda<\lambda_0$.

Figure 6 shows spectral dependences of dielectric functions for a $CuAlS_2$ platelet with thickness of 93 μm. These data indicate again on significant anisotropy of optical properties of $CuAlS_2$ crystals.

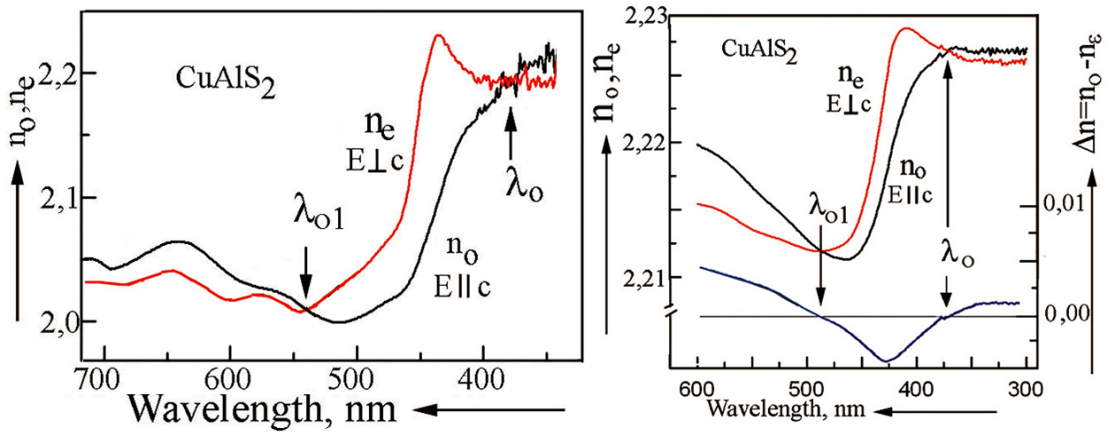

Figure 5. Spectral dependences of refractive indices for ordinary and extraordinary waves in $CuAlS_2$ crystals with thicknesses of 223 μm (left) and 35 μm (right).

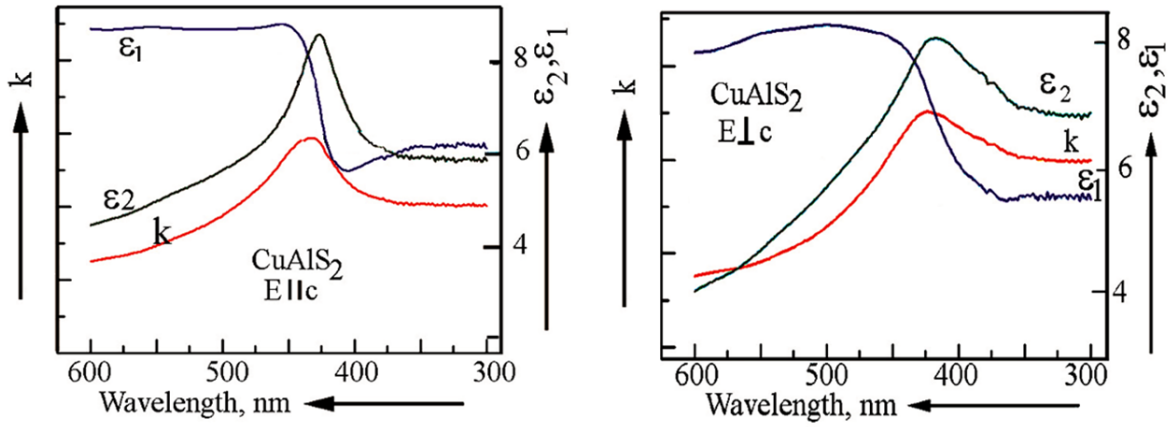

Figure 6. Spectral dependences of optical constants ε_1 ε_2, and k for polarizations E||c (left) and E⊥c (right) for $CuAlS_2$ crystals with thickness of 93 μm.

Figure 7 compares the spectral dependences of refractive indices for ordinary n_o and extraordinary n_e waves in $CuAlS_2$ crystals with thicknesses of 93 μm and 15 μm in the region of short wavelengths. Again, an isotropic wavelength is observed in both crystals around (380 – 385) nm.

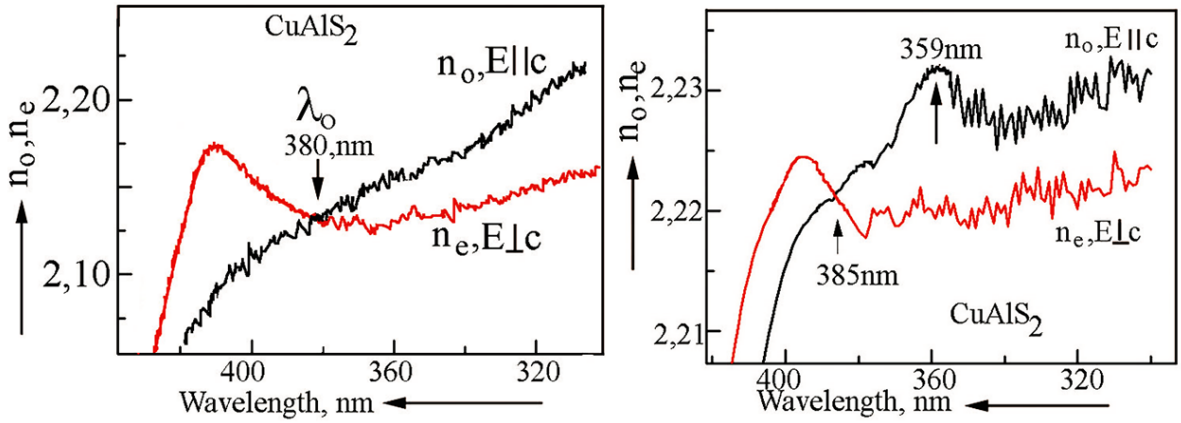

Figure 7. Spectral dependences of refractive indices for ordinary and extraordinary waves in $CuAlS_2$ crystals with thicknesses of 93 μm (left) and 15 μm (right).

If one compares the data from Figure 5 and Figure 7, one can conclude that there is no correlation between the position of the isotropic point and the crystal thickness. The variation of the isotropic point in the range of (375 – 385) nm could be due to some difference in the technological conditions of crystal growth. This suggestion is also supported by the analysis of optical properties of the crystal with thickness of 93 μm at longer wavelengths (Figure 8). In contrast to the sample with thickness of 223 nm there are practically no absorptions bands in the region of crystal transparency and the second isotropic point is absent in the 93 μm thick sample. These observations are explained by a better crystallinity and purity of this sample.

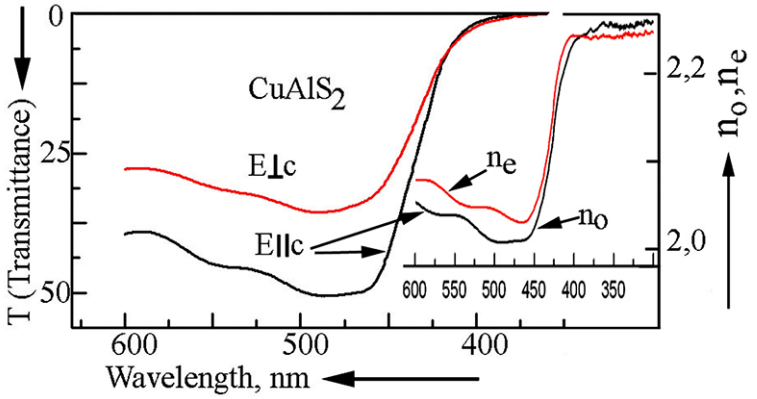

Figure8. Spectral dependences of transmission for ordinary and extraordinary waves in a $CuAlS_2$ crystal with thicknesses of 93 μm.

An optical band-pass filter was constructed from two Gran-Thompson prism polarizers and a (100) crystal plate of $CuAlS_2$ crystal with thickness of 223 μm (Figure 9). A very narrow transmission line with the full width at half maximum (FWHM) of 0.5 nm at the wavelength of λ_{01} around 535 nm is inherent to such a crystal placed between crossed polarizers.

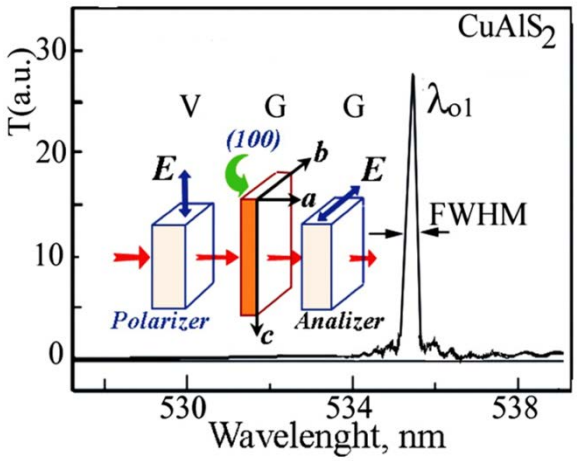

Figure 9. Transmission spectrum of $CuAlS_2$ crystals with thicknesses of 223 μm in crossed polarizers.

Conclusions

The results of this study demonstrate that strong anisotropy of optical properties and birefringence is inherent to $CuAlS_2$ single crystals. Two isotropic points were found around 380 nm and 530 nm in (100) oriented platelets. The spectral position of these isotropic points, especially for that situated around 530 nm was found to be different for platelets with different thicknesses. This difference was explained not only by the different gyroscopy in crystals with different thickness, but also by the different content and concentration of defects and impurities in crystals, which are due to different technological condition of crystal growth. An optical band-pass filter was constructed with a $CuAlS_2$ platelet with the thickness of 223 μm placed between two Gran-Thompson prism crossed polarizers. The pass band of the filter with the full width at half maximum (FWHM) of 0.5 nm is situated at 535 nm.

Acknowledgments. *The authors acknowledge financial support from the National Agency for Research and Development of the Republic of Moldova, under the project no. 20.80009.5007.20.*

References

1. Isshiki M., Wang J. Wide-band gap II-VI Semiconductors: Growth and Properties. In Kasap, S. Capper P. (eds) *Springer Handbook of Electronic and Photonic Materials*. Springer Handbooks. Springer, Cham, 2017.
2. Tamargo M.C. *II-VI Semiconductor Materials and their Applications*, CRC Press, 2002.
3. Yeh P. Zero crossing birefringent filters. In: *Optical Communication,*1980, 35, pp. 15-19.
4. Lotspeich J.F., Stephens R.R., Henderson D.M. Electrooptic tunable filters for infrared wavelengths. In: *IEEE Journal of Quantum Electronics,*1982, QE-18, pp. 1253-1258.
5. Horinaka H., Sonomura H., Miyauchi T. Optical Band-Pass Filter Using Accidental Isotropy and Optical Activity of $AgGaSe_2$, *Japanese Journal of Applied Physics*, 1985, 24, pp. 463-466.
6. Yamomoto T., Takehara H., Horinaka H., Miyauchi T. Optical Band-Pass Filter Using Accidental Isotropy and Optical Activity of $AgGaSe_2$ (II). In: *Japanese Journal of Applied Physics,*1986, 25, pp. 1397-1399.
7. Horinaka H., Yamamoto N. Optical Band-Elimination Filter Made of Optically Active Uniaxial Crystal of $AgGaSe_2$ for AlGaAs Semiconductor Laser. In: *Proceedings SPIE* 1990, 1319, pp. 592.
8. Horinaka H., Yamamoto N., Hamaguchi H. New Approach to Highly Efficient Raman Spectroscopy Using a Laser Diode and $AgGaSe_2$ Crystal Filter. In: *Applied Spectroscopy*,1992, 46, pp. 379-381.
9. Yamamoto N., Horinaka H., Cho Y., Hamaguchi H. Application of $AgGaS_2$ filter to easy Raman spectroscopy. In: *Analytical Science*, 1991, 7, pp. 581-584.
10. Susaki M., Yamamoto N., Horinaka H., Huang W.Z., Cho Y. Performance of $AgGaS_2$Crystal Filter for Raman Spectroscopy. In: *Japanese Journal of Applied Physics,* 1994, 33, pp. 1561-1564.

11. Syrbu N., Dorogan A., Ursaki V., Stamov I., Tiginyanu I. Birefringence of $CuGaS_2$ crystals. In: *Optics Communications*, 2011, 284, pp. 3552-3557.
12. Syrbu N. N., Dorogan A.V., Masnik A., Ursaki V.V. Birefringence of $CuGa_xAl_{1-x}Se_2$crystals. In: *Journal of Optics*, 2011, 13, pp. 035703(9).
13. Green M. A., Emery K., King D. L., Igari S., Warta W. Solar Cell Efficiency Tables (Version 20). In: *Progress in Photovoltaics*, 2002, 10, pp. 355-362.
14. Panthani M. G., Akhavan V., Goodfellow B., Schmidtke J. P., Dunn L., Dodabalapur A., Barbara P. F., Korgel B. A. Synthesis of $CuInS_2$, $CuInSe_2$, and $Cu(In_xGa_{1-x})Se_2$ (CIGS) Nanocrystal 'Inks' for Printable Photovoltaics, In: *Journal of the American Chemical Society*, 2008, 130(49), pp. 16770-16777.
15. Repins I., Contreras M.A., Egaas B., Dehart C., Scharf J., Perkins C. L., To B., Noufi R. 19·9% efficient ZnO/CdS/$CuInGaSe^2$ solar cell with 81·2% fill factor. In: *Progress in Photovoltaics* 2008, 16, pp. 235-242.
16. Chen B., Przdhan N., Zhong H. From Large-Scale Synthesis to Lighting Device Applications of Ternary I–III–VI Semiconductor Nanocrystals: Inspiring Greener Material Emitters. In: *The Journal of Physical Chemistry Letters*, 2018, 9, pp. 435-445.
17. Kim J. H., Yang H. High-Efficiency Cu–In–S Quantum-Dot Light-Emitting Device Exceeding 7%. In: *Chemistry of Materials*, 2016, 28, pp. 6329-6335.
18. Guijarro N., Prevot M. S., Yu X., Jeanbourquin X.A., Bornoz P., Bouree W., Johnson M., Le Formal F., Sivula K.A. Bottom-up Approach toward All-Solution-Processed High-Efficiency $Cu(In,Ga)S_2$ Photocathodes for Solar Water Splitting. In: *Advanced Energy Materials*, 2016, 6, pp. 1501949(9).
19. Fan X. B.,Yu S., Zhan F., Li Z. J., Gao Y.J., Li X.B., Zhang L.P., Tao Y., Tung C.H., Wu L.Z. Nonstoichiometric Cu_xIn_yS Quantum Dots for Efficient Photocatalytic Hydrogen Evolution. In: *ChemSusChem*, 2017, 10, pp. 4833-4838.
20. Shay J. L., Wernick J.H. *Ternary Chalcopyrite Semiconductors*. Pergamon, New York, 1975, p. 25.
21. Horinaka H., Tomii K., Sonomura H., Miyauchi T. A New Method for Measuring Optical Activity in Crystals and Its Application to Quartz. In: *Japanese Journal of Applied Physics*,1985, 24, pp. 755-760.
22. Horinaka H., Mononobe S., Yamamoto N. A criterion for Applying Chalcopyrite Semiconductors to Optical Line Elimination Filters. In: *Japanese Journal of Applied Physics*,1993, 32, pp. 109-112.
23. Levchenko S., Syrbu N. N., Tezlevan V. E., Arushanov E., Merino J.M., Leon M. Exciton spectra and energy band structure of $CuGaSe_2$ single crystals. In: *Journal of Physics D: Applied Physics*,2008, 41, pp. 055403(7).